Protein Expression and Purification 192 (2022) 106043

Contents lists available at ScienceDirect

Protein Expression and Purification

journal homepage: www.elsevier.com/locate/yprep

Antibody mimetic drug conjugate manufactured by high-yield *Escherichia coli* expression and non-covalent binding system

Kenzo Yamatsugu [a], Hiroto Katoh [b], Takefumi Yamashita [c], Kazuki Takahashi [a], Sho Aki [c], Toshifumi Tatsumi [a], Yudai Kaneko [c], Takeshi Kawamura [c,f], Mai Miura [c], Masazumi Ishii [c], Kei Ohkubo [d,e], Tsuyoshi Osawa [c], Tatsuhiko Kodama [c], Shumpei Ishikawa [b], Motomu Kanai [a], Akira Sugiyama [c,f,*]

[a] Graduate School of Pharmaceutical Sciences, The University of Tokyo, Hongo, Bunkyo-ku, Tokyo, 113-0033, Japan
[b] Department of Preventive Medicine, Graduate School of Medicine, The University of Tokyo, Tokyo, 113-0033, Japan
[c] Research Center for Advanced Science and Technology, The University of Tokyo, 4-6-1 Komaba, Meguro-ku, Tokyo, 153-8904, Japan
[d] Institute for Advanced Co-Creation Studies, Osaka University, 2-1 Yamada-oka, Suita, Osaka, 565-0871, Japan
[e] Institute for Open and Transdisciplinary Research Initiatives, Osaka University, 2-1 Yamada-oka, Suita, Osaka, 565-0871, Japan
[f] Isotope Science Center, The University of Tokyo, 2-11-16 Yayoi, Bunyo-ku, Tokyo, 113-0032, Japan

ARTICLE INFO

Keywords:
Antibody mimetic
Inclusion body
Refolding
Streptavidin

ABSTRACT

Antibody-drug conjugates (ADCs) are a major therapeutic tool for the treatment of advanced cancer. Malignant cells in advanced cancer often display multiple genetic mutations and become resistant to monotherapy. Therefore, a therapeutic regimen that simultaneously targets multiple molecules with multiple payloads is desirable. However, the development of ADCs is hampered by issues in biopharmaceutical manufacturing and the complexity of the conjugation process of low-molecular-weight payloads to biologicals. Here, we report antibody mimetic-drug conjugates (AMDCs) developed by exploiting the non-covalent binding property of payloads based on high-affinity binding of mutated streptavidin and modified iminobiotin. Miniprotein antibodies were fused to a low immunogenic streptavidin variant, which was then expressed in *Escherichia coli* inclusion bodies, solubilized, and refolded into functional tetramers. The AMDC developed against human epidermal growth factor receptor 2 (HER2) effectively killed cultured cancer cells using bis-iminobiotin conjugated to photo-activating silicon phthalocyanine. The HER2-targeting AMDC was also effective in vivo against a mouse KPL-4 xenograft model. This AMDC platform provides rapid, stable, and high-yield therapeutics against multiple targets.

1. Introduction

Developing a treatment for advanced cancer is a major problem in drug development. Targeted therapy with a definitive cytotoxic effect is necessary to eliminate disseminated malignant cancer cells. Currently, antibody-drug conjugates (ADCs) are emerging as powerful therapeutic platforms. Cytotoxic drugs, radioisotopes, or photo-activating compounds are conjugated to genetically engineered antibodies or antibody fragments to eradicate tumor cells [1].

Recombinant mammalian cells are the most used platform for the production of antibody-based therapeutics because of their ability to perform complex post-translational modifications (PTMs), which are often required for efficient secretion, improved efficacy, and stability of the drugs [2]. However, manufacturing ADCs for multiple targets and multiple payloads is hampered by difficulties in large-scale expression of mammalian proteins and problems in stable conjugation of biologicals with low-molecular-weight cytotoxic payloads [3,4].

We had previously reported a combinatorial tool kit for ADCs, developed using the streptavidin-biotin system [5]. Cupid, a low immunogenic and mutated streptavidin variant, is designed to bind bis-iminobiotin derivatives, namely, Psyche [6–9]. Previous studies have reported that Cupid can be fused to a single-chain variable fragment (scFv), effectively killing cancer cells using various payloads linked to Psyche [5]. Payloads attached to Psyche can bind Cupid owing to its high-affinity non-covalent binding properties. However, due to issues in PTMs, the yield of engineered streptavidin fused with scFv in the CHO cell expression system was low.

* Corresponding author. Research Center for Advanced Science and Technology, The University of Tokyo, 4-6-1 Komaba, Meguro-ku, Tokyo, 153-8904, Japan.
E-mail address: sugiyama@lsbm.org (A. Sugiyama).

https://doi.org/10.1016/j.pep.2021.106043
Received 20 October 2021; Received in revised form 23 December 2021; Accepted 27 December 2021
Available online 30 December 2021
1046-5928/© 2021 Elsevier Inc. All rights reserved.

Abbreviations

ADCs	antibody-drug conjugates
PTMs	post-translational modifications
scFv	single-chain variable fragment
IB	inclusion body
AMDCs	antibody mimetic-drug conjugates
SiPc	silicon phthalocyanine
IPTG	isopropyl β-D1-thiogalactopyranoside
SPR	surface plasmon resonance
SDS-PAGE	sodium dodecyl sulfate-polyacrylamide gel electrophoresis
CBB	Coomassie Brilliant Blue
FBS	fetal bovine serum

system [12].

Here, we report rapid and high-yield inclusion body (IB) expression of miniprotein antibody mimetics fused to Cupid. Monomeric fusion proteins were concentrated in the IBs of *Escherichia coli* and refolded into functional tetramers. This tetramer exhibited high-affinity binding to both target molecules, and Psyche molecules linked to payloads. Initial functional assays of antibody mimetic-drug conjugates (AMDCs) targeting EGFR (data not shown), HER2, and HER3 (data not shown) showed that the newly synthesized photo-activating silicon phthalocyanine (SiPc)-linked Psyche molecules could effectively kill cancer cells [13]. These results suggest that AMDCs using mini proteins and non-covalent attachment of selectable payloads make multi-target and multi-modality therapy possible and may be a promising platform for the development of next-generation therapeutics for advanced cancer.

2. Materials and Methods

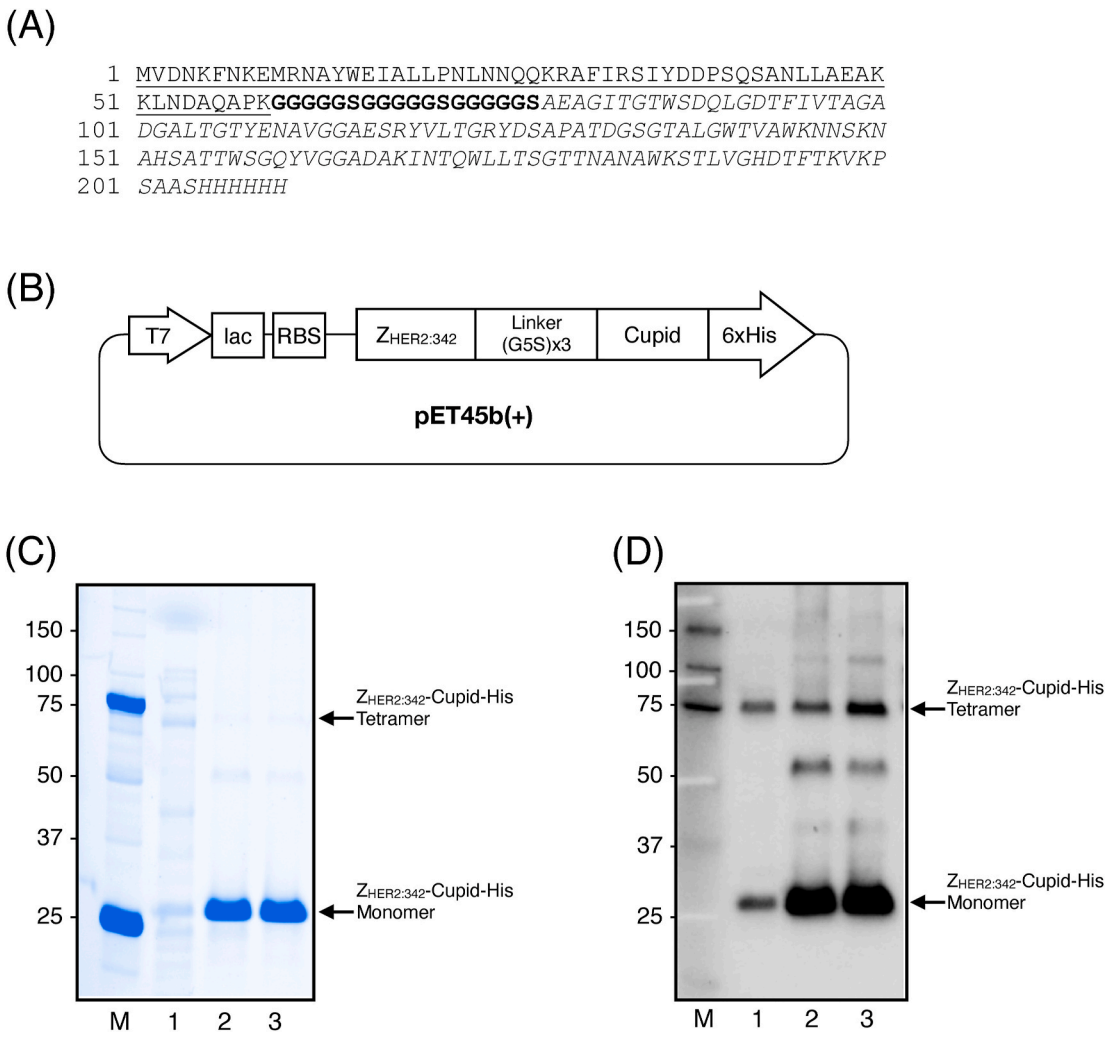

Fig. 1. Construct and analysis of protein production and antibody recognition. A. Construct of $Z_{HER2:342}$-Cupid-His in *Escherichia coli*. B. Amino acid sequence of the $Z_{HER2:342}$-Cupid-His. The $Z_{HER2:342}$ domain is underlined and the linker in bold. C. Non-reducing (no boiling and no reducing agent) SDS-PAGE analysis of $Z_{HER2:342}$-Cupid-His; lane 1, marker; lane 2, soluble fraction of the cell lysate; lane 3, insoluble fraction of the cell lysate; lane 4, washed insoluble fraction of the cell lysate. D. Western blot with anti-His Tag antibody (non-reducing).

Recently, non-immunoglobulin miniproteins (1–10 KDa) with target recognition capabilities have been reported [10,11]. These miniprotein antibody mimetics can be designed with structural and computational assistance and produced at a high yield using a bacterial expression

2.1. Materials

pET45b(+) vector was purchased from Novagen (Darmstadt, Germany). *Escherichia coli* strains DH5-Alpha and BL21(DE3) were

purchased from Nippon Gene (Tokyo, Japan). KPL-4 cells were a generous gift from Prof. Kurebayashi (Kawasaki Medical School, Kurashiki, Japan). The oligonucleotides were obtained from Eurofins Genomics (Tokyo, Japan). Carbenicillin, isopropyl β-D1-thiogalactopyranoside (IPTG), and guanidine hydrochloride were purchased from FUJIFILM Wako Chemicals (Osaka, Japan). The plasmid miniprep kit was purchased from Qiagen (GmbH, Germany) and 2xYT medium was obtained from BD Difco (Franklin Lakes, NJ).

2.2. Cloning and expression of $Z_{HER2:342}$-Cupid-His in Escherichia coli

To fuse affibody molecules and Cupid, we used the $Z_{HER2:342}$ amino acid sequence, which has been reported previously [14]. The fusion protein, $Z_{HER2:342}$-Cupid-His, was designed to combine the $Z_{HER2:342}$ and Cupid with a flexible linker $(G_5S)_3$. The cDNA of $Z_{HER2:342}$-Cupid-His was obtained from Eurofins Genomics' artificial gene synthesis service. The amino acid sequence of the expressed protein is shown in Fig. 1A. The cDNA of $Z_{HER2:342}$-Cupid-His gene was PCR-amplified with the vector provided in the artificial gene synthesis service, fused with linearized pET45b(+) expression plasmid vector using the In-Fusion HD Cloning Kit (Cat#63964, Takara Bio USA. Inc., Mountain view, CA) and transformed into DH5-Alpha competent cells (Fig. 1B). After the $Z_{HER2:342}$-Cupid-His plasmid sequencing analysis, BL21(DE3) cells were transformed with $Z_{HER2:342}$-Cupid-His plasmids and grown at 37 °C in 2 × YT broth containing 100 μg mL^{-1} carbenicillin. The medium volume was 100 mL for small-scale expression and 1 L for large-scale expression. Expression was induced with 1.0 mM IPTG at $OD_{600} = 0.8$, and the cells were cultured at 37 °C. Cells were harvested 4 h later by centrifugation (7500×*g*, 10 min, 4 °C) and stored at −80 °C.

2.3. Preparation of $Z_{HER2:342}$-Cupid-His protein

2.3.1. Isolation and purification of inclusion bodies

Cells were resuspended in lysis buffer (20 mM Tris-HCl, pH 8.0, 2 mM $MgCl_2$, 10 μg mL^{-1} lysozyme from egg white, and 2 unit/μL nuclease (Benzonase, Merck Millipore, Burlington, MA)). The suspension was sonicated using a Branson Sonifier250 (duty cycle level 2, output control level 2, 1 min; repeated three times, Hannover Germany) and incubated for 30 min at room temperature. IBs were isolated from the cell suspension by centrifugation at 12,000×*g* at 4 °C for 20 min, resuspended in washing buffer (20 mM Tris-HCl, pH 8.0), and recovered by centrifugation (12,000×*g*, 15 min at 4 °C). This process was repeated twice. The purified IBs were resuspended in water purified by reverse osmosis followed by centrifugation (12,000×*g*, 15 min at 4 °C). The purified IBs were suspended in ultra-pure water and stored in 0.5-mL aliquots in 1.5-mL tubes followed by centrifugation (12,000×*g*, 15 min at 4 °C). After centrifugation, the supernatant was discarded, and the purified IBs were stored at −80 °C.

The fraction of cell suspension, pellet of cell lysate, and purified IBs were analyzed by non-reducing (no boiling and no reducing agent) sodium dodecyl sulfate-polyacrylamide gel electrophoresis (SDS-PAGE) (TGX Stain-Free FastCast 12%, #1610185, Bio-Rad, Hercules, CA). Proteins were either stained with Coomassie Brilliant Blue (CBB) (Bullet CBB Stain One, #13542-81, Nacalai tesque, Kyoto, Japan) or transferred to a PVDF membrane using the Trans-Blot Turbo Transfer System (BIO-RAD). Immobilized proteins were incubated with 0.1 μg mL^{-1} mouse anti-His-tag mAb (Code No. D291-3, Medical & Biological Laboratories Co., Ltd., Nagoya, Japan) and detected with 0.1 μg mL^{-1} goat anti-mouse IgG-HRP (#A4416, Sigma-Aldrich, Burlington, MA) using chemiluminescent detection (SuperSignal West Pico PLUS Chemiluminescent Substrate, #34579, Thermo Scientific, Waltham, MA).

2.3.2. Denaturing and refolding

The solubilization of the IB was performed according to a previously described method [15]. Briefly, purified IBs were suspended with denaturation buffer (0.1 M Tris-HCl, pH 8.5, 10 mM EDTA, 6 M guanidine hydrochloride) and incubated on a shaker at 15 °C for 1 h followed by centrifugation (12,000×*g*, 15 min at 4 °C). After centrifugation, the supernatant was collected as solubilized $Z_{HER2:342}$-Cupid-His. The refolding of the solubilized $Z_{HER2:342}$-Cupid-His was done according to previously described methods [7,16,17]. Briefly, the solubilized $Z_{HER2:342}$-Cupid-His was diluted 40 to 50-fold with refolding buffer (0.1 M sodium phosphate, 0.4 M arginine-HCl, pH 6.0) and incubated at 4 °C for 72 h. Then, the diluted material was centrifuged (12,000×*g*, 20 min at 4 °C) to remove aggregates, and the supernatant was collected.

2.3.3. Size exclusion chromatography

The refolded $Z_{HER2:342}$-Cupid-His was analyzed by non-reducing (no boiling and no reducing agent) SDS-PAGE and quantified using absorbance at 280 nm. The supernatant was concentrated more than 10 mg/mL using an ultrafiltration unit, Vivaspin Turbo 15 PES, 30,000 MWCO (Sartorius, Göttingen, Germany). After filtering with a 0.22-μm Millex syringe filter (Merck Millipore, Burlington, MA), the resulting sample was loaded onto a gel filtration column (HiLoad 16/600 Superdex 75 pg, #28989333, Cytiva, Marlborough, MA). Size exclusion chromatography was performed with SEC buffer (0.1 M sodium phosphate, 0.2 M arginine-HCl, pH 6.5). The fractions were analyzed by non-reducing (no boiling and no reducing agent) SDS-PAGE (TGX Stain-Free FastCast 12%, #1610185, Bio-Rad, Hercules, CA). Proteins were either stained with Coomassie Brilliant Blue (CBB) stain (Bullet CBB Stain One, #13542-81, Nacalai tesque) or transferred to a PVDF membrane using the Trans-Blot Turbo Transfer System (BIO-RAD, Hercules, CA). Immobilized proteins were incubated with 0.1 μg mL^{-1} mouse anti-His-tag mAb (Code No. D291-3, Medical & Biological Laboratories Co., Ltd. Nagoya, Japan) and detected with 0.1 μg mL^{-1} goat anti-mouse IgG-HRP (#A4416, Sigma-Aldrich, Burlington, MA) using chemiluminescent detection (SuperSignal West Pico PLUS Chemiluminescent Substrate, #34579, Thermo Fisher Scientific, Waltham MA).

2.4. Synthesis of Psyche-conjugated FITC and SiPc

2.4.1. Equipment

NMR spectra were recorded on the JEOL ECX500 spectrometer, operating at 500 MHz for ^1H NMR and 124.51 MHz for ^{13}C NMR, or the JEOL ECS400 spectrometer, operating at 400 MHz for ^1H NMR and 100 MHz for ^{13}C NMR. Chemical shifts were reported in ppm on the δ scale relative to residual $CHCl_3$ ($\delta = 7.24$ for ^1H NMR and $\delta = 77.0$ for ^{13}C NMR), CHD_2OD ($\delta = 3.31$ for ^1H NMR and $\delta = 49.0$ for ^{13}C NMR). Preparative HPLC was conducted by using a JASCO HPLC system equipped with a UV-2075 spectrometer, PU-2086 pumps, a DG-2080-53 degasser, and an MX-2080-32 mixer. ESI-MS spectra were measured using Shimadzu LCMS-2020 or Agilent Technologies 6120.

2.4.2. Benzyl 14-(2-(benzyloxy)-2-oxoethyl)-2,2-dimethyl-4-oxo-3,8,11-trioxa-5,14-diazahexadecan-16-oate (**S1**)

Sodium bicarbonate (3.22 g, 38.5 mmol), potassium iodide (1.28 g, 7.70 mmol), and benzyl 2-bromoacetate (4.83 mL, 30.8 mmol) were successively added to a stirred solution of *tert*-butyl (2-(2-(2-aminoethoxy)ethoxy)ethyl)carbamate (1.91 g, 7.70 mmol) in DMF (100 mL) and the mixture was stirred at room temperature for 36 h. The reaction was quenched with 5% acetic acid solution, and the mixture was extracted with ethyl acetate. Combined organic layers were washed with water, saturated sodium bicarbonate solution, and brine, dried over sodium sulfate, filtered, and concentrated to generate crude **S1**, which was purified by silica gel column chromatography (dichloromethane/MeOH = 20:1 to 10:1) to generate **S1** (3.58 g, 6.57 mmol, y. 85%). ^1H NMR (400 MHz, $CDCl_3$) δ: 1.42 (s, 9H), 2.98 (t, 2H, $J = 5.4$ Hz), 3.26 (brt, 2H, $J = 5.4$ Hz), 3.45 (t, 2H, $J = 5.4$ Hz), 3.50 (s, 4H), 3.59 (t, 2H, $J = 5.4$ Hz), 3.68 (s, 4H), 5.11 (s, 4H), 7.30–7.35 (m, 10H); ^{13}C NMR (98 MHz, $CDCl_3$) δ: 28.1, 40.0, 53.2, 55.6, 65.9, 69.8, 69.9, 70.1, 78.8, 128.0, 128.1, 128.3, 135.4, 155.7, 170.9; LRMS (ESI): *m/z* 567 $[M+Na]^+$.

2.4.3. 14-(Carboxymethyl)-2,2-dimethyl-4-oxo-3,8,11-trioxa-5,14-diazahexadecan-16-oic acid (S2)

To a stirred solution of **S1** (131.1 mg, 240.7 μmol) in MeOH (5 mL), 10% Pd/C (24.1 mg) was added, and the mixture was stirred in a hydrogen atmosphere (balloon) at room temperature for 3 h. Argon was back filled, and the mixture was filtered through Celite. The filtrate was concentrated to generate **S2** (93.3 mg, y. quant.) as colorless syrup. ^{1}H NMR (500 MHz, CD_3OD) δ: 1.40 (brs, 9H), 3.19 (t, 2H, J = 5.2 Hz), 3.35–3.50 (m, 2H), 3.47 (t, 2H, J = 5.2 Hz), 3.58 (brs, 4H), 3.78 (m, 2H), 3.94 (brs, 4H); ^{13}C NMR (125 MHz, CD_3OD) δ: 28.8, 41.2, 56.1, 57.3, 67.1, 71.1, 71.3, 80.1, 158.5, 170.4; LRMS (ESI): *m/z* 387 $[M+Na]^+$.

2.4.4. Benzyl tert-butyl (9-(2-((4-(((benzyloxy)carbonyl)amino)butyl)amino)-2-oxoethyl)-11-oxo-3,6-dioxa-9,12-diazahexadecane-1,16-diyl) dicarbamate (S3)

To a stirred solution of **S2** (547 mg, 1.50 mmol) in DMF (15 mL), benzyl (4-aminobutyl)carbamate (834 mg, 3.75 mmol), triethylamine (1.05 mL, 7.50 mmol), and HATU (1.20 g, 3.15 mmol) were added, and the mixture was stirred at room temperature for 14 h. The reaction was quenched with 5% acetic acid solution, and the mixture was extracted with ethyl acetate. Combined organic layers were washed with brine, dried over sodium sulfate, filtered, and concentrated to generate crude **S3**, which was purified by silica gel column chromatography (dichloromethane/MeOH = 100:1 to 20:1) to obtain **S3** (1.03 g, 1.33 mmol, y. 89%). ^{1}H NMR (500 MHz, CD_3OD) δ: 1.42 (s, 9H), 1.52 (m, 8H), 3.12 (t, 4H, J = 6.3 Hz), 3.22–3.25 (m, 6H), 3.50 (t, 2H, J = 5.7 Hz), 3.57–3.66 (m, 6H), 3.73 (brs, 2H), 3.81 (brs, 4H), 5.05 (s, 4H), 7.27–7.38 (m, 10H); ^{13}C NMR (125 MHz, CD_3OD) δ: 27.4, 28.2, 28.8, 40.1, 41.2, 41.3, 56.4, 58.0, 67.3, 71.0, 71.1, 71.3, 80.1, 128.7, 128.9, 129.4, 138.4, 158.4, 158.8, 173.0; LRMS (ESI): *m/z* 773 $[M+H]^+$.

2.4.5. tert-Butyl (16-amino-9-(2-((4-aminobutyl)amino)-2-oxoethyl)-11-oxo-3,6-dioxa-9,12-diazahexadecyl)carbamate (S4)

To a stirred solution of **S3** (91.4 mg, 118.2 μmol) in MeOH (5 mL), 10% Pd/C (11.8 mg) was added, and the mixture was stirred in a hydrogen atmosphere (balloon) at room temperature for 5 h. Argon was back filled, and the mixture was filtered through Celite. The filtrate was concentrated to generate **S4** (63.3 mg, y. quant.) as colorless syrup. ^{1}H NMR (500 MHz, CD_3OD) δ: 1.40 (s, 9H), 1.57 (m, 8H), 2.75 (t, 2H, J = 5.2 Hz), 2.83 (t, 4H, J = 6.9 Hz), 3.19 (t, 2H, J = 5.7 Hz), 3.23 (t, 4H, J = 6.9 Hz), 3.26 (s, 4H), 3.48 (t, 2H, J = 5.7 Hz), 3.56–3.58 (m, 6H); ^{13}C NMR (125 MHz, CD_3OD) δ: 27.5, 28.8, 39.5, 40.9, 41.2, 55.9. 59.8, 69.9, 71.0, 71.2, 80.2, 158.5, 173.7; LRMS (ESI): *m/z* 527 $[M+H]^+$.

2.4.6. 22-((3aS,4R,6aR)-2-iminiohexahydro-1H-thieno[3,4-d]imidazole-4-yl)-9-(2-((4-(5-((3aS,4S,6aR)-2-iminiohexahydro-1H-thieno[3,4-d]imidazole-4-yl)pentanamido)butyl)amino)-2-oxoethyl)-11,18-dioxo-3,6-dioxa-9,12,17-triazadocosan-1-aminium tetra(trifluoroacetate) (S5: Psyche)

To a stirred solution of *N*-Boc iminobiotin (429.3 mg, 1.25 mmol) in DMF (10.2 mL), triethylamine (279 μL, 2.00 mmol) and carbonyldiimidazole (203 mg, 1.25 mmol) were added at room temperature [18]. The temperature was raised to 50 °C, and **S4** (252 mg, 0.500 mmol) in DMF (10 mL) was added. The mixture was stirred at 50 °C for 1 h, and 1-(3-dimethylaminopropyl)-3-ethylcarbodiimide hydrochloride (95.9 mg, 0.500 mmol) was added. The mixture was further stirred at 50 °C for 18 h, and concentrated to generate crude Boc-protected Psyche, which was purified by silica gel column chromatography (dichloromethane/MeOH = 98:2 to 70:30) to generate Boc-protected Psyche. The product was dissolved in trifluoroacetic acid/water (2:1, 20 mL) and stirred at room temperature for 1.5 h. The mixture was concentrated to generate crude **S5**, which was purified by silica gel column chromatography (reversed phase, water/acetonitrile = 95:5 to 0:100) to generate Psyche (**S5**, 276 mg, 0.21 mmol, y. 42%). ^{1}H NMR (500 MHz, CD_3OD) δ: 1.48 (dt, 4H, J = 7.5 Hz, 15.5 Hz), 1.50–1.61 (m, 10H), 1.61–1.74 (m, 4H), 1.78 (dt, 2H, J = 8.0 Hz, 15.5 Hz), 2.21 (t, 4H, J = 7.5 Hz), 2.85 (d, 2H, J = 13.1 Hz), 3.00 (dd, 2H, J = 4.6 Hz, 13.1 Hz), 3.14–3.23 (m, 6H), 3.28 (t, 4H, J = 6.3 Hz), 3.34–3.38 (m, 2H), 3.38–3.48 (m, 2H), 3.68–3.69 (m, 4H), 3.74 (t, 2H, J = 4.6 Hz), 3.80 (m, 2H), 3.96 (s, 2H), 3.98 (s, 2H), 4.54 (dd, 2H, J = 4.6 Hz, 8.1 Hz), 4.73 (dd, 2H, J = 4.6 Hz, 8.1 Hz); LRMS (ESI): *m/z* 428 $[M+2H]^{2+}$.

2.4.7. Psyche-FITC (S6)

Psyche (**S5**, 2.0 mg, 1.7 μmol) and fluorescein isothiocyanate (0.6 mg, 1.7 μmol) were mixed in DMSO-Na_2HPO_4 buffer (2:1, pH 8.4, 300 μL), and stirred at room temperature for 12 h in the dark. The mixture was diluted with 4 mL of water, and the solution was purified with reversed-phase HPLC (gradient of acetonitrile in 0.1% aqueous TFA: 0% for 5 min; 0–100% for 100 min) to generate Psyche-FITC (**S6**, 1.2 mg, 0.76 μmol, y. 45%) as light orange solid. LRMS (ESI): *m/z* 1242.65 $[M-H]^-$.

2.4.8. Psyche-SiPc (S7)

Psyche (**S5**, 1.8 mg, 1.5 μmol) and SiPc-NHS ester [19] were mixed in DMSO-Na_2HPO_4 buffer (1:1, pH 8.4, 300 μL), and stirred at room temperature for 12 h in the dark. The mixture was diluted with 1 mL of water, and the solution was purified by reversed-phase HPLC (gradient of acetonitrile in 50 mM triethylammonium acetate aqueous solution (pH 7.0): 20% for 5 min; 20–70% for 30 min) to generate Psyche-SiPc (**S7**, 1.7 mg, 0.71 μmol, y. 56%) as deep blue solid. LRMS (ESI): *m/z* 1159.20 $[M-2H]^{2-}$.

2.5. In vitro binding activity and cytotoxic activity of Her2 targeting AMDC with SiPC

2.5.1. Binding activity of $Z_{HER2:342}$-Cupid-His against HER2 and Psyche-SiPc

Surface plasmon resonance (SPR) with a Biacore T200 (Cytiva, Marlborough, MA) was used to measure the binding activity of purified $Z_{HER2:342}$-Cupid-His. HER2 extracellular domain (R&D SYSTEMS, Minneapolis, MN) were covalently coupled to a CM5 chip according to the manufacturer's instructions (Cytiva, Marlborough, MA). Subsequently, purified $Z_{HER2:342}$-Cupid-His (2-fold dilution series from 4.267E-8 to 6.667E-10 M) was used to assess sensor interaction. By systematically analyzing antigen-$Z_{HER2:342}$-Cupid-His binding and dissociation, affinity dissociation constant (KD) values were calculated using Biacore T200 Evaluation Software version 3. In the same way, the interaction between $Z_{HER2:342}$-Cupid-His and Psyche-SiPc was analyzed using Biacore T200. Purified $Z_{HER2:342}$-Cupid-His was covalently coupled to a CM5 chip according to the manufacturer's instructions (Cytiva, Marlborough, MA). Subsequently, Psyche-SiPc molecule (2-fold dilution series from 10.000E-9 to 0.625E-9 M) was used to assess sensor interaction. By systematically analyzing $Z_{HER2:342}$-Cupid-His vs. Psyche-SiPc binding and dissociation, KD values were calculated using Biacore T200 Evaluation Software version 3.

2.5.2. In vitro cell assays

2.5.2.1. Cell line. The KPL-4 cell line was maintained in DMEM (low glucose) (FUJIFILM Wako Chemicals Corporation, Osaka, Japan) supplemented with 10% fetal bovine serum (FBS), 100 U mL^{-1} penicillin, and 100 μg mL^{-1} streptomycin (#15140122, Thermo Fisher Scientific, Waltham MA) [19].

2.5.2.2. Internalization analysis. KPL-4 cells were seeded at a cell density of 5.0×10^4 cells/well on glass-bottom dishes (35 mm Glass based dish, #3971-035, Iwaki, Shizuoka, Japan). Cells were washed with pre-warmed starvation medium (serum-free medium) twice and incubated at 37 °C for 1 h. The cells were placed on ice in a 4 °C cold room for 15 min to block endocytosis. To form a complex, $Z_{HER2:342}$-Cupid-His and Psyche-FITC (S6) were mixed in a molar ration of 1:2 in the dark, on ice

for 10 min. The medium was replaced with ice-cold starvation medium containing 10 μg mL^{-1} of the complex. Next, cells were incubated at 4 °C for 30 min to label HER2 on the cell surface and washed twice with ice-cold starvation medium. The cells were then moved to a 37 °C incubator for various durations (0, 1, 24 h) to allow for internalization of the complex. To remove proteins that were bound non-specifically to the cell surface, the cells were washed with 2 mL ice-cold stripping buffer (pH 4.6 citrate buffer) at 4 °C for 2 min on ice and then briefly washed with ice-cold phosphate-buffered saline (PBS) [20]. Next, the cells were fixed with fixation buffer (4% paraformaldehyde) on ice for 15 min and rinsed with PBS. Then, the cells were counterstained with DAPI and rinsed with PBS again.

2.5.2.3. Confocal imaging. The cells were excited sequentially frame by frame at 408 nm and 488 nm, with the detection set to 500–535 nm. Fluorescence was observed through a 63 × 1.40 NA oil immersion objective (HC PL APO 63 × /1.40 Oil CS2, Leica). Lightning Mode (Leica Microsystems, Wetzlar, Germany) was used to generate deconvolved images. Microscope acquisitions were controlled by LAS X (v. 4.2.1) software from Leica [21].

2.5.2.4. In vitro phototoxicity studies. The effect of Psyche-SiPc (S7)-conjugated $Z_{HER2:342}$-Cupid-His on tumor viability was assessed using cell counting kit-8 (CCK-8) (Code No. CK40, Dojindo Laboratories, Kumamoto, Japan) as previously described [13]. Briefly, 1 × 10^3 cells per well with 50 μL of medium were seeded in 96-well plates and cultured overnight. To induce complex formation between $Z_{HER2:342}$-Cupid-His and Psyche-SiPc, $Z_{HER2:342}$-Cupid-His and Psyche-SiPc were mixed in a molar ratio of 1:2 in the dark, on ice for 10 min. Subsequently, the cells were separately incubated for 24 h at 37 °C in 50 μL of different concentrations of $Z_{HER2:342}$-Cupid-His-SiPc complex, which were prepared by ten-fold sequential dilution from 20 μg mL^{-1}. Then, the drug-containing medium was removed, the cells were washed with PBS once, and fresh media was added. The cells were irradiated from the bottom of the 96-well plate with 690 nm LED light (Yamato Scientific Co., Ltd., Tokyo, Japan) at 100 J cm^{-2} at room temperature. After 24 h, 10 μL of CCK-8 reagent was added per well, the plates were incubated at 37 °C for 1.5 h, and absorbance was measured at 450 nm using a microplate reader (iMark, BIO-RAD, Hercules, CA) [13]. Blank wells (culture medium and CCK-8 reagent) and control wells (untreated cells, culture medium, and CCK-8 reagent) were also measured.

2.6. Animal experiments

2.6.1. Animals and photoactivation therapy in vivo

This study was approved by the Institutional Animal Care and Use Committee (Permission number: RAC210005) and carried out according to the University of Tokyo Animal Experimentation Regulations. KPL-4 cells (7.5 million) were transplanted subcutaneously into the thigh of BALB/cSlc-nu/nu nude mice (Sankyo Labo Service Corporation, Inc. Tokyo, Japan). Subcutaneous tumor growth was monitored by measuring tumor volume (0.5 × length × $width^2$) using a caliper. Animal body weight was monitored as an indicator of treatment-related toxicity. Tumors in the three mice ranged from approximately 500 mm^3–800 mm^3 48 days after cell implantation. Tumor volumes were measured twice a week after a single i.v. injection of 150 μg $Z_{HER2:342}$-Cupid-His-SiPc complex. Twenty hours post-injection of the $Z_{HER2:342}$-Cupid-His complex, the tumors were irradiated with 690 nm LED light (Yamato Scientific Co., Ltd., Tokyo, Japan) at 230 J cm^{-2} under anesthesia [5]. Forty-eight hours after the first irradiation, the tumors were irradiated again in the same way. One of the three mice was dissected 14 days after the second irradiation. The other two mice were dissected 36 days after the second irradiation.

2.6.2. Pathological analysis after photoactivation therapy in vivo

Tissues resected from the mice as mentioned above were fixed with 4% paraformaldehyde phosphate buffer solution (#163–20145, FUJIFILM Wako Pure Chemical Corporation, Osaka, Japan) for 24 h at 4 °C and then embedded in paraffin according to standard histopathological procedures. Hematoxylin-eosin staining (H.E. staining) was performed as described below. Histopathological specimens of the tissues were deparaffinized by immersion in xylene (#241-00091, FUJIFILM Wako Pure Chemical Corporation, Osaka, Japan) for 10 min at room temperature; then rehydrated by immersing in ethanol (#057–00451, FUJIFILM Wako Pure Chemical Corporation, Osaka, Japan). Hematoxylin (#6187-4P, Sakura Finetek Japan, Tokyo, Japan) and eosin (#8660, Sakura Finetek Japan, Tokyo Japan) solutions were used to perform H.E. staining according to the manufacturer's protocols. Finally, stained slides were dehydrated by immersion in ethanol and xylene. The slides were then covered with glass coverslips using Marinol (#4197193, Muto Pure Chemicals, Tokyo, Japan). The H.E.-stained slides were histopathologically examined using the OLYMPUS cellSens Standard system (OLYMPUS, Tokyo, Japan).

3. Results and discussion

3.1. $Z_{HER2:342}$-Cupid-His expression and purification from inclusion bodies

3.1.1. Construction of the vector

To obtain a recombinant $Z_{HER2:342}$-Cupid-His protein, $Z_{HER2:342}$ was fused with Cupid using a $(Gly\text{-}Gly\text{-}Gly\text{-}Gly\text{-}Gly\text{-}Ser)_3$ flexible linker (Fig. 1A). Based on the amino acid sequence, cDNA was artificially synthesized. The gene was sub-cloned into linearized pET45b(+) (Fig. 1B). DNA sequencing results (data not shown) showed that the recombinant plasmid was correctly constructed.

3.1.2. Expression of $Z_{HER2:342}$-Cupid-His in Escherichia coli BL21 (DE3)

We succeeded in expressing a large amount of affibody molecules in IBs of *Escherichia coli* after IPTG induction (Fig. 1C). Expression and recovery of IBs is an effective expression method in *Escherichia coli* [15]. Since affibody molecules do not form disulfide bonds and do not have mammalian sugar chains, they can be expressed in large amounts in IBs by fusion to Cupid from actinomycetes. The recombinant $Z_{HER2:342}$-Cupid-His monomer contains 210 amino acids, and the expected molecular weight is 21.79 kDa. Protein expression was induced with 1 mM IPTG at 37 °C. After a 4-h culture, recombinant $Z_{HER2:342}$-Cupid-His was detected only in the insoluble fraction as IBs by SDS-PAGE under non-reducing (no boiling and no reducing agent) conditions (Fig. 1C). On the other hand, monomeric and tetrameric forms (~80 kDa) were detected by Western blot analysis under non-reducing (no boiling and no reducing agent) conditions with anti-His tag antibody in both the soluble fraction and IBs (Fig. 1D). There was not much difference between unwashed IBs (Fig. 1C and D, lane 2) and washed IBs (Fig. 1C and D, lane 3). Washing the $Z_{HER2:342}$-Cupid-His IBs with simple Tris-HCl buffer, followed by two washes with ultra-pure water to reduce the contaminants, was found to be sufficient to produce high-purity IBs. The cells were cultured in 2.5-L flasks with 1 L of medium for 4 h at 37 °C after induction by IPTG, and approximately 1 g (wet weight) of IBs was purified.

3.2. Renaturation of $Z_{HER2:342}$-Cupid-His from Escherichia coli inclusion bodies and gel filtration column chromatography

Various methods have been experimented with for the refolding of antibody fragments [22]. Refolding chemically denatured proteins into correctly folded and biologically active conformations presents a significant technical challenge. Generally, many conditional studies need to be conducted to determine the optimal buffer condition that promotes proper refolding [22]. Since $Z_{HER2:342}$-Cupid-His did not contain

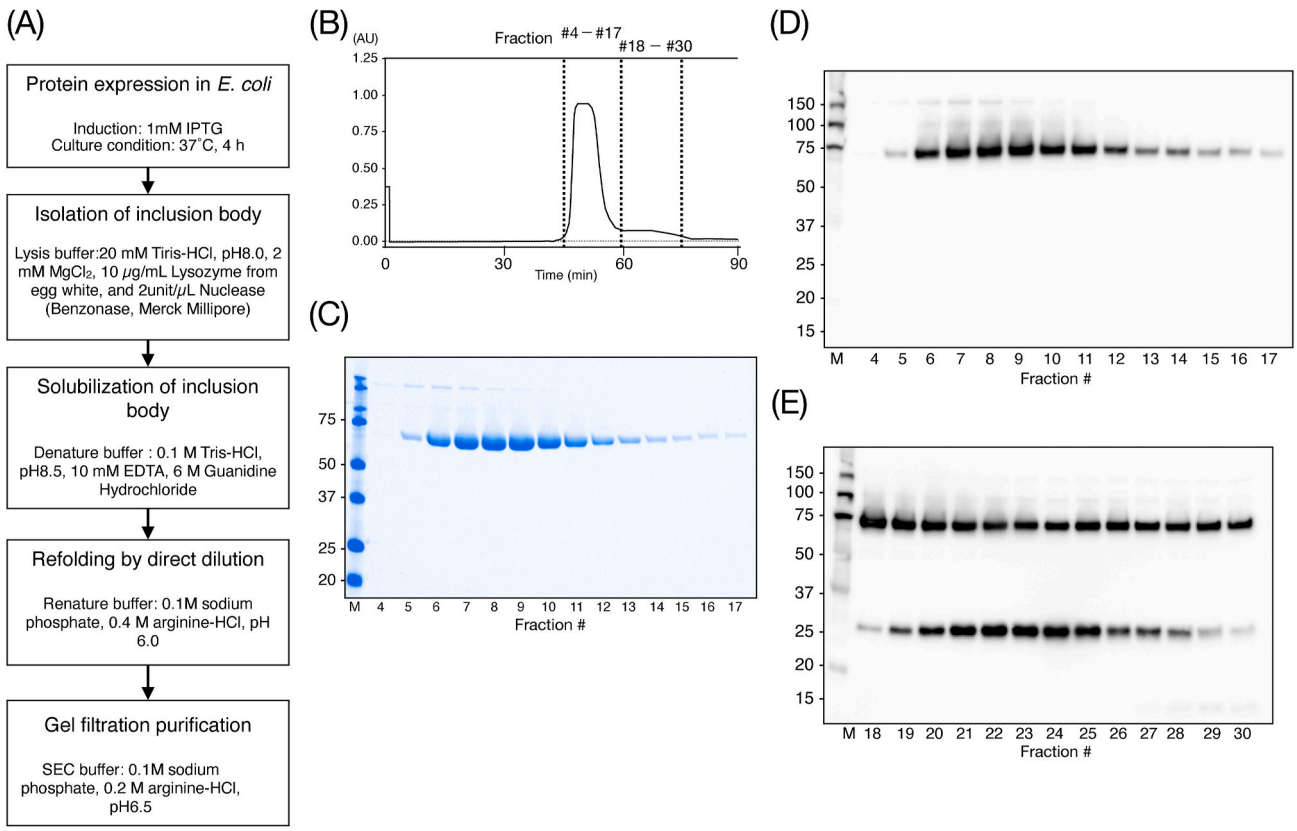

Fig. 2. Purification of recombinant $Z_{HER2:342}$-Cupid-His from IBs. A. Procedure for production of active recombinant $Z_{HER2:342}$-Cupid-His. B. Gel filtration purification chromatograms. C. Non-reducing (no boiling and no reducing agents) SDS-PAGE analysis of $Z_{HER2:342}$-Cupid-His purification fractions. Lanes 1, molecular weight marker (kDa); lane 2–14, fraction from #4 to #17. Because of the high sensitivity of western blotting, the samples were diluted 100-fold. D. Western blot of fraction #4–17 with anti-His tag antibody (non-reducing). E. Western blot of fraction #18–30 with anti-His tag antibody (non-reducing).

cysteine residues, there was no need to use a complex buffer, including reducing or oxidizing agents, to reconstitute the disulfide bond. The renaturing process was performed using a relatively simple renaturation buffer (Fig. 2A).

The theoretical isoelectric point (pI) of recombinant monomeric $Z_{HER2:342}$-Cupid-His was calculated to be approximately 7.1. However, the pI of the $Z_{HER2:342}$ domain and Cupid-His domain were calculated as 9.1 and 6.45, respectively. To prevent the inhibition of tetramer formation by intra- or intermolecular contact due to electric charge, the refolding buffer used was phosphate buffer including 0.4 M arginine to prevent aggregation at pH 6.0, to lend a positive charge to both $Z_{HER2:342}$ and Cupid-His domains (Fig. 2A).

After refolding by direct dilution of chemically denatured 220 mg of IBs, 78 mg of soluble protein was obtained. After 1 h of refolding, non-reducing (no boiling and no reducing agent) SDS-PAGE revealed that the sample contained a mixture of monomers and tetramers. However, after 72 h, SDS-PAGE confirmed that more than 90% of the identified bands were tetramer bands (data not shown). The refolded sample was concentrated and purified by gel filtration chromatography. In the buffer used for gel filtration chromatography, the arginine concentration was reduced to 0.2 M for cell assay and animal experiments (Fig. 2A). The chromatogram showed one prominent UV peak (fraction #4–17) and one small UV peak (fraction #18–30) (Fig. 2B). The high purity of tetrameric $Z_{HER2:342}$-Cupid-His was confirmed in fractions #4–17 by CBB staining and Western blot analysis (Fig. 2C and D). However, Western blot analysis of fractions #18–30 showed that these fractions contained both tetrameric and monomeric $Z_{HER2:342}$-Cupid-His (Fig. 2E).

After gel filtration purification, an average of 35 mg of tetrameric $Z_{HER2:342}$-Cupid-His was obtained from 220 mg of IBs in three-time experiments. The estimated total yield of purified tetrameric $Z_{HER2:342}$-Cupid-His was 160 mg per liter. In our previous experiments, average yield of anti-CEA-scFv-Cupid was 0.356 mg per liter, and average yield of anti-HER2-scFv-Cupid was 0.163 mg per liter [5]. The yield of $Z_{HER2:342}$-Cupid-His was 500–1000 times higher than that of scFv conjugated cupid proteins.

3.3. Analysis of Her2 binding and ligand binding by SPR

To confirm the bifunctional binding ability of $Z_{HER2:342}$-Cupid-His, binding ability analyses were performed on the HER2 extracellular domain and Psyche-SiPc molecule using Biacore T200. To evaluate the affinity of $Z_{HER2:342}$-Cupid-His for HER2, recombinant HER2 extracellular domain (HER2-ECD) was immobilized on a Biacore Series S Sensor Chip CM5 and subjected to kinetic analysis by injecting $Z_{HER2:342}$-Cupid-His (Fig. 3A). The K_D value of $Z_{HER2:342}$-Cupid-His vs. HER2-ECD was established to be in the low-to sub-picomolar range, which was calculated to be approximately 256 pM (Fig. 3A). To confirm the affinity between $Z_{HER2:342}$-Cupid-His and Psyche-SiPc, $Z_{HER2:342}$-Cupid-His was immobilized on Sensor Chip CM5 and subjected to kinetic analysis by injecting Psyche-SiPc using single-cycle kinetics mode (Fig. 3B). The K_D value of $Z_{HER2:342}$-Cupid-His vs. Psyche-SiPc was approximately 569 pM (Fig. 3B). The synthesized tetramer binds with high avidity to the recombinant Her2 extracellular domain by virtue of being tetravalent when bound to Cupid, despite its large molecular weight.

3.4. Internalization assay

Whether or not the antibody is internalized after binding is an important factor in selecting a payload; for example, for anticancer drug

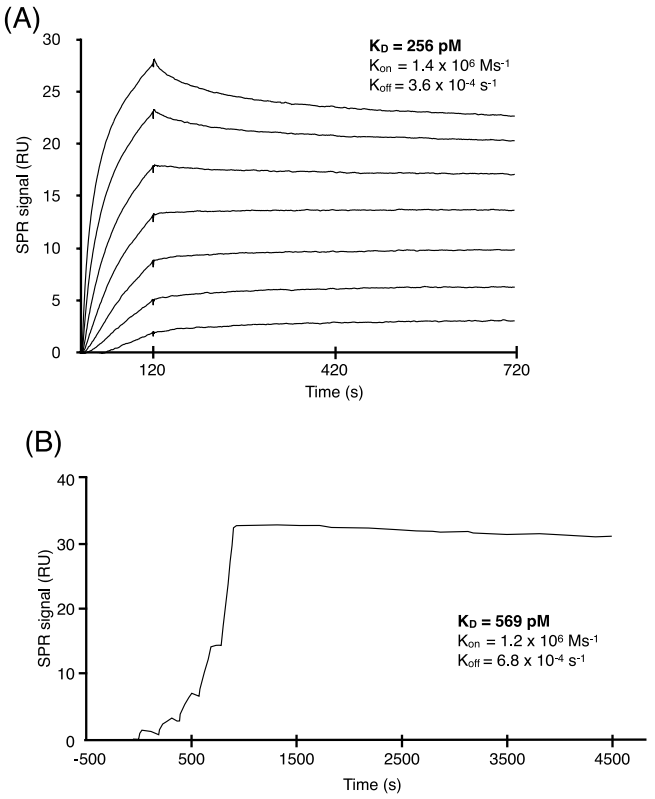

Fig. 3. $Z_{HER2:342}$-Cupid-His biding analysis against antigen HER2 extracellular domain and Psyche-SiPc by Biacore T200. A. Affinity analysis of $Z_{HER2:342}$-Cupid-His and HER2 extracellular domain protein. B. Affinity analysis of $Z_{HER2:342}$-Cupid-His and Psyche-SiPc compound. The structure of Psyche-SiPc is shown in the Materials and Methods section as **S7**.

payloads used in ADCs, internalization is necessary [23]. On the other hand, in cases such as pre-targeting radioimmunotherapy, it is desirable that it remains on the cell surface [24]. Therefore, we tested whether ZHER2:342-Cupid-His could be internalized after cell binding.

$Z_{HER2:342}$-Cupid-His was pre-conjugated with Psyche-FITC and 10 μg mL^{-1} of $Z_{HER2:342}$-Cupid-His-Psyche-FITC was added to the cells. Fig. 4 shows that $Z_{HER2:342}$-Cupid-His-Psyche-FITC binds efficiently to the surface of Her2-expressing cancer cells. As reported in previous studies, slow internalization was observed (Fig. 4) [20]. Even though the cells were washed with acidic buffer, pictures show that many molecules were present on the cell surface, suggesting that the use of payloads that function on the cell surface would be effective. It is also a suitable platform for isotope therapy by pre-targeting radioimmunotherapy [24]. On the other hand, it is also recognized that payloads are internalized after a long time, and there is a possibility that the utility will be further expanded with improvements in the future.

3.5. *Cytotoxicity of $Z_{HER2:342}$-Cupid-His•Psyche-SiPc complex*

We examined the response of KPL-4 cells to the complex of $Z_{HER2:342}$-Cupid-His and Psyche-SiPc irradiated with visible light at 690 nm. Psyche-SiPc and $Z_{HER2:342}$-Cupid-His were conjugated at a 2:1 M ratio. KPL-4 cells were incubated with medium containing 1 × 10^{-5}–10 μg mL^{-1} of the complex. After incubation for 24 h, cells were washed and cultured in fresh medium, and irradiated with visible light at 690 nm, at 100 J cm^{-2}. KPL-4 cells were killed by light irradiation in a drug-concentration-dependent manner, whereas no such phenomenon was

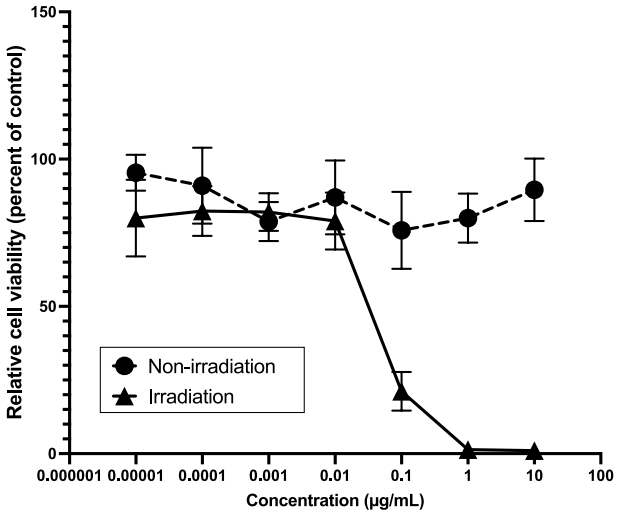

Fig. 5. Cytotoxicity of $Z_{HER2:342}$-Cupid-His. $Z_{HER2:342}$-Cupid-His and Psyche-SiPc were conjugated before addition to cells. KPL-4 cells were cultured with medium containing the complex of $Z_{HER2:342}$-Cupid-His and Psyche-SiPc for 24 h, and then the drug-containing medium was removed. The cells were washed with PBS twice and cultured with a fresh medium following irradiation. The graph represents results obtained after 24 h of incubation as assayed by 690 nm light irradiation (▲ solid triangle) or non-irradiation (● solid circle). Data points represent mean ± SD.

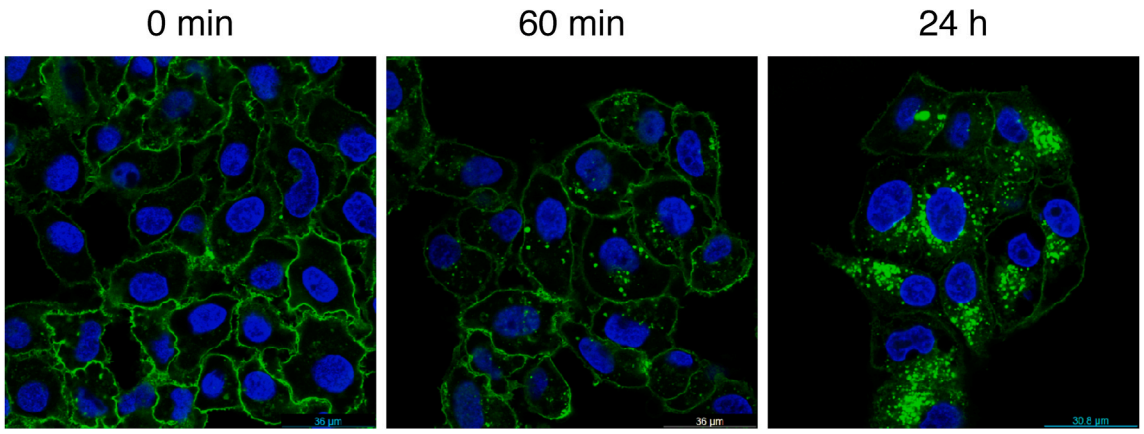

Fig. 4. Confocal image cell surface retention of $Z_{HER2:342}$-Cupid-His with Psyche-FITC. The structure of Psyche-FITC is shown in the Materials and Methods section as **S6**. $Z_{HER2:342}$-Cupid-His and Psyche-FITC were pre-conjugated before addition to cells. Cells were incubated with the medium containing 10 μg mL^{-1} pre-conjugated complex of $Z_{HER2:342}$-Cupid-His and Psyche-FITC at 4 °C for 30 min. Then, cells were incubated at 37 °C for 1 or 24 h.

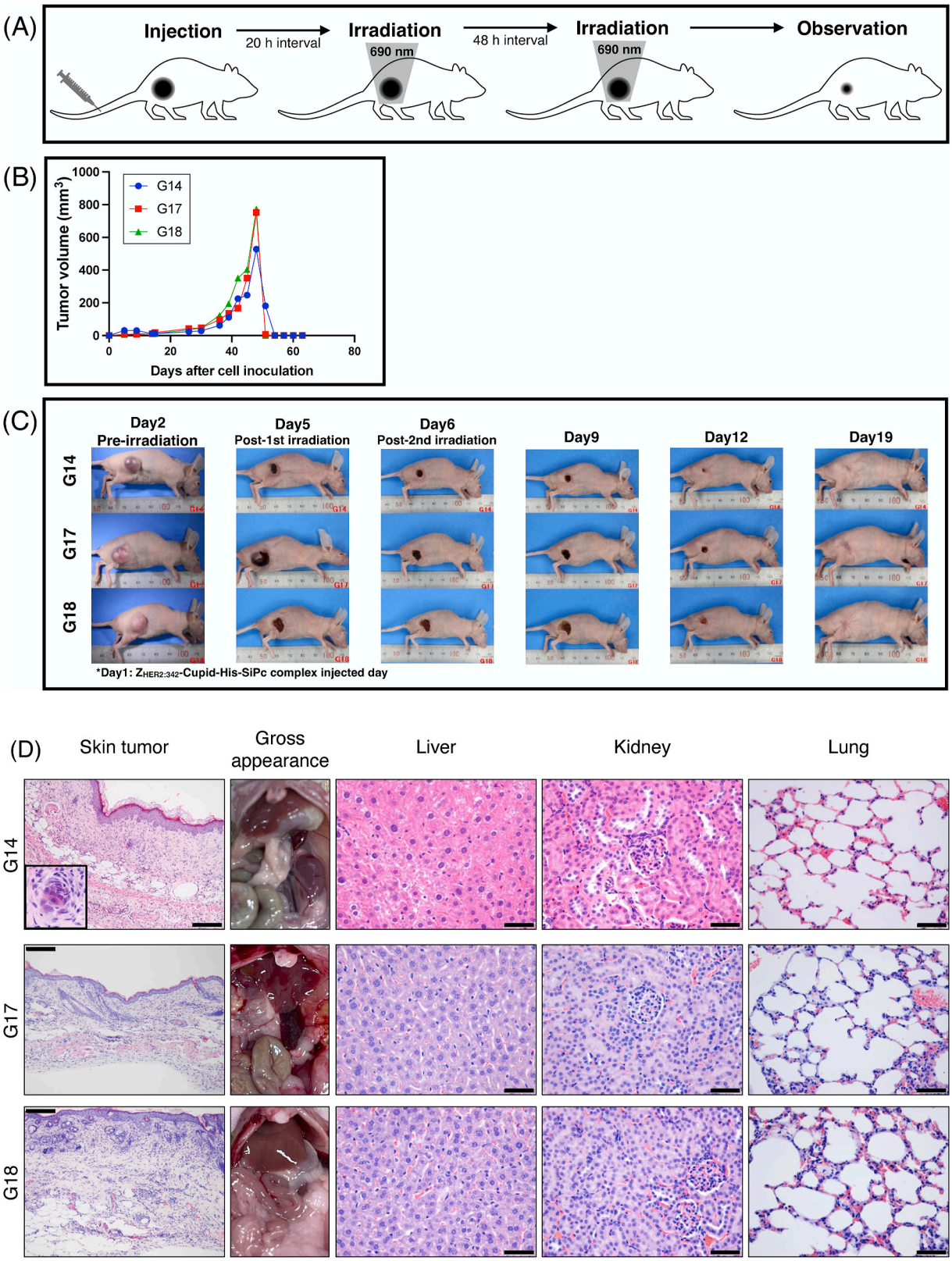

Fig. 6. Effects of tumor eradication by the $Z_{HER2:342}$-Cupid-His-Psyche-SiPc complex in vivo. A. A schematic outline of the animal experiment. B. The graph shows the change in tumor volume after KPL-4 implantation. C. Effect of Psyche-SiPc-conjugated $Z_{HER2:342}$-Cupid-His on the KPL-4 xenograft. D. Histopathological examinations of the skin tissues and major organs of the eradicated mice shown in Fig. 6D, which used to harbor subcutaneous tumors. Histologically, the eradicated skin tissues were replaced by fibrous regenerative tissues with nearly no obvious viable tumor cells (left panels), except for the G14 mouse, in which a small cluster of tumor cells was found in the fibrous skin, although they did not seem to be viable (cropped picture in the left-upper panel). The gross appearances of the major organs did not show any obvious pathological features in the eradicated mice, which was confirmed by histological examinations. Other organs such as the heart, alimentary tract, pancreas, spleen, and brain did not show obvious pathologies in these mice (data not shown). Black scale bars in the pictures indicate 100 μm and 50 μm for the skin tissues and other organs, respectively.

observed in the absence of light irradiation (Fig. 5).

3.6. Tumor eradication effects of the $Z_{HER2:342}$-Cupid-His•Psyche-SiPc complex in vivo

To examine the effect of Psyche-SiPc-conjugated $Z_{HER2:342}$-Cupid-His on KPL-4 xenograft mice, we carried out the experiments shown in the schematic outline of Fig. 6A. The mice received 150 μg of $Z_{HER2:342}$-Cupid-His-SiPc complex and were exposed to 690 nm light at 230 J cm^{-2} under anesthesia approximately 20 h later [5]. They were further exposed to the same conditions for 48 h (Fig. 6A). The size of the tumor mass, which was approximately 300–500 mm^3 before the test, dramatically decreased after light irradiation (Fig. 6B and C). After the first 48 h of light exposure, a darkened appearance was observed, suggestive of hemorrhagic necrosis. After the second light exposure, the tumor was further reduced in size. On the 19th day after drug administration and the 18th day after the first light irradiation, the wounds in the area where the tumor had necrosed had completely healed (Fig. 6C). Histological examination of the mice confirmed the high efficacy of the treatment. The eradicated skin tissues were almost completely replaced with fibrous regenerative tissues with nearly no viable tumor cells, except in the case of the G14 mouse, where a small cluster of tumor cells remained in the fibrous skin (Fig. 6D). The remaining tumor cells did not seem fully viable; thus, it can be concluded that the eradication effects of the $Z_{HER2:342}$-Cupid-His-SiPc complex were substantially high in vivo. Notably, both gross appearance and histopathological examination of major organs revealed no obvious pathological side effects in the treated mice (Fig. 6D). Recently, ADCs targeting HER2 have been shown to be toxic to hepatocytes [25]. As a payload, our novel photosensitizer caused no liver, kidney, or lung pathology (Fig. 6D).

4. Conclusion

In this study, we describe an antibody mimetic-drug conjugate (AMDC) using the Cupid and Psyche system for the treatment of cancers. Based on the mutant streptavidin (Cupid) and iminobiotin (Psyche) system, the design and manufacturing methodology of Cupid fused with antibody mimetic mini proteins and Psyche linked to photosensitizer SiPc were established.

The refolding and purification of ZHER2:342-Cupid-His can be completed in less than a week, and high-purity ZHER2:342-Cupid-His required for cell-level and animal studies can be produced in units of several hundred milligrams. High-purity ZHER2:342-Cupid-His enables direct dilution of solubilized IBs into the refolding buffer without prior purification under denaturing conditions. In addition, the complex of ZHER2:342-Cupid-His and Psyche-SiPc, which was pre-bound *in vitro*, demonstrated a tumor-reducing effect at 690 nm light irradiation in a xenograft mouse model.

In conclusion, the methods established in this study and the results obtained will provide an important platform for the development of therapeutics against advanced cancers.

Declaration of interest

K.Y., T.Y., K.T., T.T., T.K., M.K., and A.S. are coinventors on a patent application that incorporates discoveries described in this manuscript. T.K. and A.S. are cofounders of Savid Therapeutics.

Author contributions

Kenzo Yamatsugu: Resources, Writing-Reviewing, and Funding acquisition, Hiroto Katoh: Methodology, Data curation, and Funding acquisition, Takefumi Yamashita: Software, Kazuki Takahashi: Resources, Aki Sho: Methodology, Toshihumi Tatsumi: Resources, Yudai Kaneko: Analysis, Takeshi Kawamura: Analysis, Mai Miura: Resources and Validation, Masazumi Ishii: Resources, Kei Ohkubo: Supervision, Tsuyoshi Osawa: Methodology, Tatsuhiko Kodama: Conceptualization, Writing-original draft, Editing and Project administration, Shumpei Ishikawa: Supervision, Motomu Kanai: Supervision, Akira Sugiyama: Conceptualization, Writing-Reviewing, Editing, Project administration, and Funding acquisition.

Acknowledgments

Funding: This work was supported by JSPS KAKENHI, Japan [grant number JP21392851 to Akira Sugiyama]; the Japan Agency for Medical Research and Development (AMED), Japan [grant number JP20ck0106414 to Tatsuhiko Kodama]; AMED, Japan [grant number JP21am0401010 to Shumpei Ishikawa]; AMED, Japan [grant number JP21ak0101096 to Hiroto Katoh]; and Takeda Science Foundation, Japan to Kenzo Yamatsugu.

References

[1] M.L. Chiu, D.R. Goulet, A. Teplyakov, G.L. Gilliland, Antibody structure and function: the basis for engineering therapeutics, Antibodies 8 (2019) 55, https://doi.org/10.3390/antib8040055.
[2] N. Jenkins, L. Murphy, R. Tyther, Post-translational modifications of recombinant proteins: significance for biopharmaceuticals, Mol. Biotechnol. 39 (2008) 113–118, https://doi.org/10.1007/s12033-008-9049-4.
[3] R. Yang, T. Jain, H. Lynaugh, R.P. Nobrega, X. Lu, T. Boland, I. Burnina, T. Sun, I. Caffry, M. Brown, X. Zhi, A. Lilov, Y. Xu, Rapid assessment of oxidation via middle-down LCMS correlates with methionine side-chain solvent-accessible surface area for 121 clinical stage monoclonal antibodies, mAbs 9 (2017) 646–653, https://doi.org/10.1080/19420862.2017.1290753.
[4] X. Lu, R.P. Nobrega, H. Lynaugh, T. Jain, K. Barlow, T. Boland, A. Sivasubramanian, M. Vasquez, Y. Xu, Deamidation and isomerization liability analysis of 131 clinical-stage antibodies, mAbs 11 (2019) 45–57, https://doi.org/10.1080/19420862.2018.1548233.
[5] A. Sugiyama, T. Kawamura, T. Tanaka, H. Doi, T. Yamashita, K. Shinoda, H. Fujitani, K. Yamatsugu, Y. Shimizu, T. Tatsumi, K. Takahashi, M. Kanai, E. Mizohata, T. Kawato, T. Doi, T. Inoue, T. Kodama, Cupid and Psyche system for the diagnosis and treatment of advanced cancer, Proc. Jpn. Acad. Ser. B Phys. Biol. Sci. 95 (2019) 602–611, https://doi.org/10.2183/pjab.95.041.
[6] T. Kawato, E. Mizohata, T. Meshizuka, H. Doi, T. Kawamura, H. Matsumura, K. Yumura, K. Tsumoto, T. Kodama, T. Inoue, A. Sugiyama, Crystal structure of streptavidin mutant with low immunogenicity, J. Biosci. Bioeng. 119 (2015) 642–647, https://doi.org/10.1016/j.jbiosc.2014.10.025.
[7] K. Yumura, M. Ui, H. Doi, T. Hamakubo, T. Kodama, K. Tsumoto, A. Sugiyama, Mutations for decreasing the immunogenicity and maintaining the function of core streptavidin, Protein Sci. 22 (2013) 213–221, https://doi.org/10.1002/pro.2203.
[8] T. Kawato, E. Mizohata, Y. Shimizu, T. Meshizuka, T. Yamamoto, N. Takasu, M. Matsuoka, H. Matsumura, T. Kodama, M. Kanai, H. Doi, T. Inoue, A. Sugiyama, Structure-based design and synthesis of a bivalent iminobiotin analog showing strong affinity toward a low immunogenic streptavidin mutant, Biosci. Biotechnol. Biochem. 79 (2015) 640–642, https://doi.org/10.1080/09168451.2014.991692.
[9] T. Kawato, E. Mizohata, Y. Shimizu, T. Meshizuka, T. Yamamoto, N. Takasu, M. Matsuoka, H. Matsumura, T. Kodama, M. Kanai, H. Doi, T. Inoue, A. Sugiyama, Structure-based design of a streptavidin mutant specific for an artificial biotin analogue, J. Biochem. 157 (2015) 467–475, https://doi.org/10.1093/jb/mvv004.
[10] X.W. Yu, Y.P. Yang, E. Dikici, S.K. Deo, S. Daunert, Beyond antibodies as binding partners: the role of antibody mimetics in bioanalysis, Annu. Rev. Anal. Chem. 10 (2017) 293–320, https://doi.org/10.1146/annurev-anchem-061516-045205.
[11] J. Lofblom, F.Y. Frejd, S. Stahl, Non-immunoglobulin based protein scaffolds, Curr. Opin. Biotechnol. 22 (2011) 843–848, https://doi.org/10.1016/j.copbio.2011.06.002.
[12] Z.R. Crook, N.W. Nairn, J.M. Olson, Miniproteins as a powerful modality in drug development, Trends Biochem. Sci. 45 (2020) 332–346, https://doi.org/10.1016/j.tibs.2019.12.008.
[13] K. Takahashi, A. Sugiyama, K. Ohkubo, T. Tatsumi, T. Kodama, K. Yamatsugu, M. Kanai, Axially substituted silicon phthalocyanine payloads for antibody-drug conjugates, Synlett 32 (2021) 1098–1103, https://doi.org/10.1055/a-1503-6425.
[14] C. Eigenbrot, M. Ultsch, A. Dubnovitsky, L. Abrahmsen, T. Hard, Structural basis for high-affinity HER2 receptor binding by an engineered protein, Proc. Natl. Acad. Sci. U.S.A. 107 (2010) 15039–15044, https://doi.org/10.1073/pnas.1005025107.
[15] R.R. Burgess, Refolding solubilized inclusion body proteins, Methods Enzymol. 463 (2009) 259–282, https://doi.org/10.1016/S0076-6879(09)63017-2.
[16] L.H. Chua, S.C. Tan, M.W.O. Liew, Process intensification of core streptavidin production through high-cell-density cultivation of recombinant *E. coli* and a temperature-based refolding method, J. Biotechnol. 276–277 (2018) 34–41, https://doi.org/10.1016/j.jbiotec.2018.04.012.
[17] A. Mirzadeh, G. Saadatnia, M. Golkar, J. Babaie, R. Noordin, Production of refolded *Toxoplasma gondii* recombinant SAG1-related sequence 3 (SRS3) and its use for serodiagnosis of human toxoplasmosis, Protein Expr. Purif. 133 (2017) 66–74, https://doi.org/10.1016/j.pep.2017.03.001.
[18] T. Suzuki, Y. Totani, M. Kosuke, S. Banba, H. Kamada, T. Nakayama, H. Akiba, K. Tsumoto, T. Inoue, Method for Identifying Drug-Discovery Target Protein for

Development of Antibody Drug, and Method for Producing Antibody against Target Protein, WO2018151301A1, 2019.
[19] J. Kurebayashi, T. Otsuki, C.K. Tang, M. Kurosumi, S. Yamamoto, K. Tanaka, M. Mochizuki, H. Nakamura, H. Sonoo, Isolation and characterization of a new human breast cancer cell line, KPL-4, expressing the Erb B family receptors and interleukin-6, Br. J. Cancer 79 (1999) 707–717, https://doi.org/10.1038/sj.bjc.6690114.
[20] H. Wallberg, A. Orlova, Slow internalization of anti-HER2 synthetic affibody monomer 111In-DOTA-ZHER2:342-pep2: implications for development of labeled tracers, Cancer Biother. Radiopharm. 23 (2008) 435–442, https://doi.org/10.1089/cbr.2008.0464.
[21] S. Aki, K. Yoshioka, N. Takuwa, Y. Takuwa, TGFbeta receptor endocytosis and Smad signaling require synaptojanin1, PI3K-C2alpha-, and INPP4B-mediated phosphoinositide conversions, Mol. Biol. Cell 31 (2020) 360–372, https://doi.org/10.1091/mbc.E19-11-0662.
[22] T. Arakawa, D. Ejima, Refolding Technologies for antibody fragments, Antibodies 3 (2014) 232–241, https://doi.org/10.3390/antib3020232.
[23] C. Chalouni, S. Doll, Fate of antibody-drug conjugates in cancer cells, J. Exp. Clin. Cancer Res. 37 (2018) 20, https://doi.org/10.1186/s13046-017-0667-1.
[24] O.C. Boerman, F.G. van Schaijk, W.J. Oyen, F.H. Corstens, Pretargeted radioimmunotherapy of cancer: progress step by step, J. Nucl. Med. 44 (2003) 400–411.
[25] Y. Endo, N. Mohan, M. Dokmanovic, W.J. Wu, Mechanisms contributing to ado-trastuzumab emtansine-induced toxicities: a gateway to better understanding of ADC-associated toxicities, Antib. Ther. 4 (2021) 55–59, https://doi.org/10.1093/abt/tbab005.